Water Research 302 (2026) 126099

Contents lists available at ScienceDirect

Water Research

journal homepage: www.elsevier.com/locate/watres

Advancing continuous in-situ quantification of microbial contamination in environmental waters using tryptophan-like fluorescence—Sensor design and validation

Whitney Knopp [a,b], Joshua Klaus [a], Danny Wilson [b], Michael J. Vlah [b], Matthew R.V. Ross [b,c], Evan Thomas [a,b,*]

[a] University of Colorado Boulder, 4001 Discovery Drive, Suite N290, Boulder, CO, 80303, USA
[b] Virridy, Boulder, CO, USA
[c] Department of Ecosystem Science and Sustainability, Colorado State University, Fort Collins, CO, USA

ARTICLE INFO

Dataset link: https://github.com/SweetSenseInc/lume_natural_waters_paper

Keywords:
Microbial water quality
Tryptophan-like fluorescence
Continuous monitoring
In-situ sensing
Recreational waters
Fecal contamination

ABSTRACT

Microbial contamination of recreational and source waters poses persistent public health risks, yet conventional monitoring based on laboratory culture methods provides delayed results and limited temporal resolution. These constraints hinder timely identification of short-duration contamination events and effective management of recreation advisories. This study evaluates the performance of a continuous, in-situ tryptophan-like fluorescence (TLF) monitoring system for high-frequency assessment of microbial water quality across laboratory experiments, site-specific field deployments, and a global multi-site modeling framework. Site-specific analyses employed conventional linear regression, while a machine learning approach was used to develop a global model trained across multiple deployments and evaluated using temporal holdouts.

Under controlled laboratory conditions, the system reproducibly demonstrated sub-ppb sensitivity that exceeds the stated detection limits of many commercially available TLF instruments. Field deployments in recreational surface waters showed strong agreement between sensor-derived *Escherichia coli* estimates and laboratory measurements obtained using the industry-standard Colilert method. Approximately 75% of linear, continuous predictions fell within the analytical uncertainty bounds of Colilert with a mean absolute percentage error of 7% in log-transformed concentration space. Binary classification at management-relevant thresholds for a deployment on the Seine in Paris achieved a balanced accuracy of greater than 90% for time-blocked test holdout data. A global model demonstrated a mean absolute percentage error of approximately 19% on temporally held-out test data in log space. Quantitative agreement was strongest at moderate to high concentrations, with increased uncertainty at low concentrations reflecting limitations of both fluorescence sensing and culture-based reference methods.

Together, these results demonstrate that continuous TLF-based measurement can complement laboratory monitoring by providing real-time screening and decision support for recreational water management. As additional deployments and training data are incorporated, the global model is expected to further improve, enhancing the scalability and operational value of continuous microbial water quality monitoring.

1. Introduction

Microbial contamination of surface waters remains a persistent public health challenge, particularly in rivers, lakes, and coastal environments used for recreation. Exposure during swimming, wading, boating, and other water-based activities is a well-established pathway for gastrointestinal illness and other adverse health outcomes, with risks often driven by short-duration contamination events that are poorly resolved by conventional monitoring approaches (Collier et al., 2021). Despite substantial investments in wastewater and stormwater infrastructure, fecal contamination of recreational waters continues to occur across both high- and low-income regions worldwide.

In many regions, recreational water quality is influenced by complex and dynamic sources, including combined sewer overflows (CSOs), wastewater treatment plant discharges, failing onsite wastewater systems, stormwater runoff, and diffuse inputs from wildlife and agricultural activities (Walker et al., 2019; Verhougstraete and Sexton, 2015;

* Corresponding author at: University of Colorado Boulder, 4001 Discovery Drive, Suite N290, Boulder, CO, 80303, USA.
E-mail address: ethomas@colorado.edu (E. Thomas).

https://doi.org/10.1016/j.watres.2026.126099
Received 18 February 2026; Received in revised form 10 April 2026; Accepted 9 May 2026
Available online 15 May 2026

Benjamin et al., 2013). These inputs often result in rapid, episodic increases in microbial contamination following precipitation events or infrastructure failures. Because routine monitoring programs rely primarily on periodic grab sampling and laboratory-based culture methods, advisory decisions are frequently made 24–48 h after exposure has already occurred, limiting their effectiveness for protecting public health (WHO, 2003; Craun et al., 2005).

Recreational and natural waters therefore represent a critical use case where high-frequency, real-time information is essential. Managers must balance the need to rapidly identify hazardous conditions against the risk of unnecessary closures that restrict access and erode public trust. This challenge is further intensified by climate-driven increases in the frequency and intensity of extreme precipitation, which are expected to amplify microbial loading and increase the temporal variability of contamination in surface waters.

These constraints have motivated growing interest in continuous, in-situ approaches to microbial water quality monitoring that can complement laboratory methods by providing real-time or near-real-time indicators of contamination. Tryptophan-like fluorescence (TLF) provides a direct optical measurement of microbial-associated fluorophores present in water and has been linked to fecal contamination in surface waters influenced by wastewater and stormwater inputs. While prior studies have demonstrated the promise of TLF for screening contamination risk, questions remain regarding low-end sensitivity, quantitative agreement with laboratory reference methods, reproducibility across fluorimeters, and suitability for operational decision-making (Ward et al., 2020; Sorensen et al., 2015).

In this study, we evaluate the performance of a continuous TLF-based monitoring system using controlled laboratory experiments, site-specific field deployments, and a global multi-site modeling framework focused on recreational and source water environments. We assess quantitative agreement with laboratory *Escherichia coli* measurements, categorical classification at management-relevant thresholds, sensitivity relative to existing TLF instrumentation, and sensor-to-sensor consistency across deployments. We further examine how partner agencies use real-time microbial data to inform recreation advisories and communicate risk to the public. Together, the results demonstrate how continuous fluorescence-based measurements can address critical temporal gaps in recreational water monitoring and support more timely, risk-informed management of surface waters.

2. Background

Although the importance of microbial water quality monitoring is well established, persistent gaps in data — particularly high-frequency water quality information — continue to limit effective protection of public health (Hope, 2024). These gaps are especially consequential for surface waters, where microbial contamination exhibits pronounced spatial and temporal variability driven by precipitation events, wastewater infrastructure dynamics, and diffuse watershed inputs (van Vliet et al., 2023; Jones et al., 2023, 2024; Schilling et al., 2009; Harmel et al., 2006). As a result, episodic contamination events that pose acute exposure risks are often poorly characterized by conventional monitoring programs.

Regular monitoring of recreational and source waters for fecal contamination is required for regulatory compliance in the United States and Europe, including under frameworks such as the Clean Water Act and the EU Bathing Water Directive (Tiwari et al., 2021). However, these programs typically rely on periodic grab sampling and laboratory-based analysis, which provide limited temporal resolution and often deliver results only after exposure has already occurred. This mismatch between monitoring frequency and contamination dynamics constrains the ability of agencies to issue timely advisories, assess the effectiveness of mitigation measures, or communicate risk clearly to the public.

Water quality data are therefore not only essential for regulatory reporting, but also for operational decision-making and public communication. In recreational settings, access to timely and interpretable water quality information supports decisions related to beach closures and reopenings, event-based advisories, and prioritization of confirmatory sampling. Previous research has shown that access to water quality information increases the likelihood of protective behaviors and risk mitigation actions by both individuals and institutions (Trent et al., 2018; Jalan and Somanathan, 2008; Hamoudi et al., 2012; Okyere et al., 2017). However, the value of such information depends critically on its timeliness and the capacity of agencies to act on it.

In high-income countries, water quality monitoring is routinely used for treatment process control and validation and compliance assessment (EPA, 2016). Extending these principles to recreational waters requires monitoring approaches capable of capturing rapid changes in microbial conditions and supporting near-real-time decision-making. Continuous, high-frequency measurements have the potential to address these limitations by filling temporal data gaps, improving situational awareness during dynamic conditions, and enabling more responsive and transparent management of recreational water quality.

2.1. Conventional microbial monitoring methods

Fecal and microbial contamination is measured with fecal indicator bacteria (FIB), the most widely accepted FIB for freshwater are *Escherichia coli* (*E. coli*) and thermotolerant coliforms (TTCs) (WHO, 2022). Traditional *E. coli* monitoring consists of grab sampling in the field, laboratory analysis with culture- or enzyme-based methods and enumeration following an incubation period; contamination is quantified in colony-forming units (CFU) or most probable number (MPN) per 100 mL of water (EPA, 2012; European Parliament and Council of the European Union, 2006). Membrane filtration and Colilert/Coliert-18 Quanti-Tray are laboratory-based methods that comply with U.S. EPA and International Standards Organization (ISO) regulations, recognized by the World Health Organization (WHO) and used by the European Union (Tiwari et al., 2021; ISO, 2012). Other laboratory methods for enumeration of *E. coli* include polymerase chain reaction (PCR) tests, DNA probe assays, absorption spectroscopy, fluorescence-based and fluorescence spectroscopy methods, flow cytometry and a range of biofluorimeters (Offenbaume et al., 2020). While considered the standard for *E. coli* enumeration and monitoring, these laboratory-based methods are significantly limited. They require travel to collect samples, highly trained personnel, costly equipment and consumables, and culture-based methods necessitate incubation times of 18+ hours. Recognizing such limitations, in 2019, UNICEF released a target product profile (TPP) of technologies for rapid *E. coli* detection; no product to date has been able to meet the stringent requirements for time to result, cost and sensitivity/specificity (UNICEF, 2023). Field test kits, like those from Aquagenics (www.aquagenx.com) and portable labs have improved accessibility to testing and accurate enumeration or presence/absence of microbial contamination in water systems. However, results produced by these methods provide only a single snapshot of water quality, twenty four hours after a sample is taken and analyzed, often not representative of the safety of an entire water source. Field and lab-based monitoring methods have limited ability to provide spatially explicit and temporally dense water quality data, preventing timely actions for the protection of public health.

2.2. Tryptophan-like fluorescence as a measurement of fecal contamination

Fluorescence-based sensing has emerged as a complementary approach to traditional culture-based methods for assessing microbial contamination in water (Ward et al., 2021; Sorensen et al., 2015). Tryptophan-like fluorescence (TLF) refers to the optical measurement of compounds that fluoresce at the characteristic excitation/emission wavelength pair (approximately 280/350 nm) associated with the aromatic amino acid tryptophan. These fluorophores are intrinsic components of microbial cells and their metabolic byproducts, and their presence in water reflects microbial-associated organic material derived

Fig. 1. The fluorimeter technology deployed in Boulder Creek, Colorado. A typical installation includes the fluorimeter (at right in gold), an enclosure anchored on the shore (left), a wired antenna if the unit is fully submerged, and complemented by sampling and enumeration (center). Photograph is unedited; individuals pictured provided consent for publication. (For interpretation of the references to color in this figure legend, the reader is referred to the web version of this article.)

from fecal inputs and subsequent biological activity (Jariyasopit and Khoomrung, 2023). As such, TLF represents a direct physicochemical measurement of microbial-associated fluorescence in water, rather than an indirect surrogate or substitute for microbiological enumeration.

A substantial body of literature has demonstrated strong associations between TLF intensity and fecal contamination in groundwater and surface waters, including correlations with thermotolerant coliforms and *Escherichia coli* (Sorensen et al., 2015; Khamis et al., 2015). Because TLF can be measured continuously, reagentlessly, and in situ, it is particularly well suited for real-time or near-real-time monitoring applications. Previous studies have therefore characterized TLF as an effective indicator of general microbial activity and as a high-frequency screening measurement for fecal contamination risk (Sorensen et al., 2018, 2020; Ward et al., 2021; Nowicki et al., 2019). However, a single, globally transferable relationship between TLF intensity and laboratory-based enumeration of *E. coli* has not been identified, reflecting both the diversity of TLF sources and the fundamental differences between optical and culture-based measurements.

Culture-based methods quantify fecal contamination through biological growth or enzymatic activity under controlled laboratory conditions. The Colilert method enumerates *E. coli* and total coliforms using defined substrates that target β-glucuronidase and other specific enzymes, yielding a most probable number (MPN) estimate after incubation (Adams et al., 1990; Rice et al., 0000). In contrast, membrane filtration methods for thermotolerant (fecal) coliforms rely on the physical capture of bacteria on a filter followed by incubation on selective media at elevated temperatures, producing colony-forming unit (CFU) counts (EPA, 2023). These approaches differ in analytical mechanism, target organisms, and sensitivity to environmental stressors, but both represent standardized measurements of viable indicator organisms associated with fecal contamination.

TLF measurements differ fundamentally in that they quantify the instantaneous fluorescence signal arising from microbial biomass and associated organic compounds present in the water at the time of measurement, regardless of organism viability or culturability. Studies have shown that a substantial fraction of measured TLF is extracellular, with reported losses of 32%–86% following filtration through 0.2 μm membranes in surface waters (Baker et al., 2007), and approximately 97% of TLF in groundwater attributed to extracellular sources (Sorensen et al., 2020). These findings underscore that TLF captures a broader representation of microbial-associated material than culture-based methods, which are inherently restricted to organisms capable of growth under specific laboratory conditions.

TLF measurement, Colilert-based *E. coli* enumeration, and membrane filtration for thermotolerant coliforms should be understood as different but complementary approaches to measuring fecal contamination in water. Each method interrogates a distinct aspect of the same underlying process — the presence and dynamics of fecal-derived microbial material — over different timescales and through different physical, chemical, and biological mechanisms. Differences among these measurements therefore reflect methodological scope and sensitivity rather than disagreement about contamination itself. Environmental factors such as temperature and turbidity can influence fluorescence intensity through changes in quantum yield and optical quenching and must be addressed through calibration and correction (Khamis et al., 2015). When appropriately interpreted, TLF provides a direct, high-frequency measurement that complements laboratory-based enumeration by capturing transient contamination dynamics that are often missed by episodic sampling.

3. Methods

In this paper, we present hardware and analytical design, and laboratory and field based evaluation of a new TLF-based fecal contamination sensor, the Lume (Fig. 1), developed by Virridy (www.virridy.com/lume).

3.1. System design

3.1.1. Mechanical

The fluorimeter integrates a compact opto-electronic core within a waterproof IP67-rated housing designed for long-term deployment in aquatic environments (Fig. 2). Mechanically, the assembly centers on a sealed optical head that aligns the excitation source, optical filters, and detector along a fixed optical axis. Precision-mounted lenses and O-ring interfaces provide both optical stability and environmental isolation. Internal baffles and the optical window geometry are configured to minimize stray light and internal reflections while maintaining a short, well-defined measurement path length. The housing consists of concentric structural elements that physically separate the wetted optical interface from the electronics cavity. This architecture supports reliable sealing, simplifies serviceability, and provides protection against fouling and mechanical shock. Bayonet-style mechanical interfaces allow

Fig. 2. Fluorimeter mechanical, electrical and optical assembly.

the optical head and enclosure components to be disassembled for maintenance without disturbing internal optical alignment. Electrically, the excitation source, photodetector, and analog front-end circuitry are tightly integrated to support stable and repeatable fluorescence measurements. A secondary electronics module manages power regulation, data acquisition, and communications.

3.1.2. Excitation

Fluorescence excitation is provided by two high-power ultraviolet light-emitting diodes (LEDs) with a nominal peak wavelength of 273 nm. The LEDs exhibit spectral bandwidths of approximately 262–290 nm at greater than 10% of peak output and 255–308 nm at greater than 1% of peak output. Each LED produces approximately 19 mW of radiant power at a forward current of 120 mA. The LEDs are driven using a linear-current LED driver based on a switching regulator topology to minimize heat generation and power consumption, thereby extending battery life. The driver provides 4096 discrete current levels, enabling fine control of excitation intensity. Because the LED radiant flux exhibits a nonlinear relationship with forward current, comparisons across operating currents account for this behavior. Component tolerances, process variation, and temperature and aging coefficients affect the LEDs, driver circuitry, and current-setting resistors. The current range set resistor is a 0.1% precision component with a temperature coefficient of 25 ppm $°C^{-1}$. To mitigate thermal effects, the measurement algorithm employs 100 μs excitation pulses with a 1 ms cycle time, limiting LED self-heating and reducing temperature-dependent drift.

3.1.3. Sample chamber

Excitation light passes through a sapphire optical window into the sample chamber, where photons interact with the aqueous sample, including dissolved organic matter, particulates, air bubbles, and chamber walls. The chamber geometry and surface finishes are designed to prevent external light leakage and provide a consistent internal reflection coefficient at relevant wavelengths. Fluorescent emission reaching the detection window passes through an optical bandpass filter selected to strongly attenuate excitation wavelengths below 300 nm (optical density ≥6) while transmitting more than 70% of light near 350 nm. Air bubbles at the detection window can alter photon incident angles and reduce filter effectiveness; therefore, a surface coating was selected to reduce bubble adhesion and persistence.

3.1.4. Emission detection

Fluorescent emission is detected using a silicon photomultiplier (SiPM) array. Behind the bandpass filter, this signal is therefore largely tryptophan-like fluorescence (TLF). By adjusting the bias voltage applied to the SiPM, the detector can operate across regimes ranging from single-photon sensitivity to average light intensity measurement. A dedicated switching voltage regulator generates and controls the SiPM bias voltage. The regulator includes dual current mirrors that monitor SiPM current. Bias voltage is measured by the microcontroller using a 12-bit analog-to-digital converter (ADC) and controlled via a 12-bit digital-to-analog converter (DAC). Both ADC and DAC reference a discrete voltage regulator with accuracy better than 0.1% across expected operating temperatures and device aging. Precision 0.1% resistors are used throughout the bias monitoring and control circuitry to minimize thermal and long-term drift. Due to device-to-device process variation and temperature dependence, per-unit calibration of the SiPM bias circuitry as a function of temperature is required.

3.1.5. Turbidity

The fluorimeter incorporates a compact time-of-flight (TOF) optical sensor that provides water presence detection, user safety, and turbidity sensing. The TOF emits short pulses of near-infrared light centered at approximately 940 nm, a wavelength commonly used by optical turbidity sensors, and measures the time-resolved return signal from the optical path. This signal is used to verify whether the measurement chamber is submerged, ensuring that fluorescence measurements are only reported when water is present. This also provides a user safety feature — if the optical cap is opened or the chamber is exposed, the firmware will prevent the UV LEDs from operating.

Increases in particulate concentrations produce stronger and more diffuse backscatter at 940 nm, which is captured as changes in return intensity and signal shape. As a result, the TOF sensor provides a turbidity signal. These turbidity-related metrics are used both to provide contextual water quality information and to identify periods when optical attenuation or scattering may influence tryptophan-like fluorescence measurements.

3.1.6. Temperature

The fluorimeter includes a temperature sensor co-located in the optical head. Temperature is a useful water quality parameter inherently, while also used in the algorithm to compensate for temperature dependence of the electronics as well as inherent fluorescence.

3.1.7. Measurement algorithm

Each measurement cycle begins with a sweep of SiPM bias voltages while the optical chamber is dark. The resulting current measurements are used to characterize dark current, noise behavior, and SiPM breakdown voltage at the prevailing temperature. Following dark characterization, the LED driver is activated and swept across a defined range of excitation currents. During each excitation cycle, SiPM current is sampled at 3.2 MHz from both current monitors. Immediately prior to each ultraviolet pulse, the SiPM current is averaged over a 64 μs interval to characterize the dark baseline. Near the end of each excitation pulse, the current is averaged over a 16 μs interval to capture fluorescence during the most stable illumination period. Data from sixteen excitation cycles are averaged to compute the final measurement values. Minimum and maximum values observed during each cycle are retained to

estimate measurement variability, which primarily reflects dark current noise and, at lower bias voltages, discrete photon detection events. Measurements across the range of SiPM bias voltages and LED currents are transmitted via the cellular network to a cloud-based service. Calibration parameters specific to each instrument are applied server-side to compute calibrated fluorescence measurements for downstream analysis.

3.2. Tryptophan response

Sensor response to tryptophan was measured at concentrations of 0.1, 0.5, 1, 10 and 50 ppb tryptophan. This range is inclusive of findings proposed by Sorensen et al. (2018) whereby TLF thresholds of 1.3, 2.4, 6.9 and 27.1 ppb align with low, medium, high and very high risk waters, as defined by the World Health Organization (WHO). Three fluorimeters were immersed in a plastic basin filled with 5 L of DI water. The basin was progressively dosed with 100 ppm or 100 ppb stock tryptophan solutions to achieve test concentrations and mixed for 15 min prior to the data collection period of 15 min. Stock 100 ppm solution was prepared by mixing 0.1 g powdered L-tryptophan (Sigma Aldrich reagent grade L-tryptophan) into 1 L of Type I ultrapure deionized (DI) water for 30 min on a stir plate, inverting for 30 s at the 15 min interval. The 100 ppb solution was prepared as a serial dilution of 100 ppm stock. The procedure tested solutions in order of increasing tryptophan concentration. The lowest calibration standard (0.1 ppb tryptophan in deionized water) produced a statistically significant normalized fluorescence response across all three sensors ($p = 0.0002$, linear regression), establishing an empirical detection threshold below 0.1 ppb. Reliable quantification with consistent inter-sensor agreement was observed from approximately 0.5 ppb. These values represent empirical sensitivity thresholds based on the calibration series rather than formal limits of detection or quantification computed using the 3σ/slope method, as the calibration design was intended to characterize sensor linearity across the environmentally relevant concentration range.

3.3. Turbidity response

Impacts of turbidity on both the TLF and TOF sensors response were tested with a constant, known tryptophan concentration and varying turbidity. One liter of 60 ppb tryptophan was mixed according to the aforementioned procedure of serial dilution. Tryptophan/turbidity solutions of 30 ppb tryptophan were made by mixing 100 mL of 60 ppb tryptophan (0 NTU) solution and 100 mL of lab-grade turbidity standard (Hach StablCal) (0 ppb). Turbidity concentrations varied at 0.5, 5, 10, 50, 100 and 500 NTUs. StablCal standards are composed of stabilized formazin, a synthetic polymer suspension that produces uniform, repeatable light scattering; these standards do not replicate the optical properties of natural suspended sediments such as silt or clay, and the sensor's turbidity response under natural sediment loads may differ from the results reported here. Tryptophan was held constant at 30 ppb after the first two tests (DI/0 NTU and DI/0.2 NTU). Following the same method of spiking the test basin, fluorimeters were immersed in 5 L of DI water and tested for 15 min at each turbidity. Solutions were tested in order of increasing turbidity, beginning with 0 NTU/30 ppb tryptophan. Exact turbidity was measured with a bench turbidimeter (Hach 2100N Laboratory Turbidimeter) at the end of each 15-minute test period, prior to the next spike.

3.4. Microbial enumeration

Laboratory-enumerated *E. coli* concentrations were developed for the training and validation of the regression and machine learning models. Grab sampling collocated with each sensor installation site was performed. Samples were collected downstream and as close to the fluorimeter as possible, stored in 250 mL polypropylene bottles, placed in a cooler during transport from the field and were processed in the lab within 2 h of collection. mWater (www.mwater.co), a mobile survey tool was used to log and store the time and location of sampling data. The date and time of sensor installation, cleaning and battery replacement events were also recorded in mWater. Membrane filtration (MF) and Colilert were used to enumerate *E. coli* and concentrations were averaged between the two methods as ground truth data. A total of 661 samples were taken across 12 sites. Negative controls (sterile DI water blanks) were processed alongside experimental samples at regular intervals to verify the absence of laboratory contamination and confirm assay specificity.

For MF, 100 mL of 10:1 sample to DI water dilutions were filtered through 0.45 μm filters, plated on S-endoagar plates and incubated at 35 C for 24 +/− 2 h (EPA, 2023; ISO, 2014). *E. coli* were enumerated after incubation by counting the number of dark, shiny coliforms under a backlit magnifying glass and multiplying the count by 10 to obtain units of CFU/100 mL. Each sample was plated in triplicates and *E. coli* counts averaged. Enumeration data for *E. coli* coliforms were recorded in mWater.

The IDEXX Quanti-Tray/2000 system with Colilert reagent (IDEXX Laboratories, Westbrook, ME; www.idexx.com) was used to enumerate *E* coli; the system delivers semiautomated quantification based on the Most Probable Number (MPN) model and is a US EPA approved analytical method for quantification of *E. coli* (EPA, 2018; U.S. Environmental Protection Agency, 2024). 100 mL of water sample is poured into an IDEXX vessel and Colilert reagent is added. Samples are centripetally mixed, poured into a Quanti-Tray and sealed with the Quanti-Tray sealer. Trays are incubated for 24 ± 2 h at 35 °C. The MPN *E. coli* concentration is the number of large and small wells, using the reference matrix, that are yellow and fluorescent under UV light. *E. coli* MPN data were recorded in mWater. At each combination of small and large wells, IDEXX provides upper- and lower-bound values at 95% confidence for the MPN/100 mL estimate. These manufacturer-provided 95% confidence intervals were used to define the analytical uncertainty bounds against which sensor predictions were compared; a prediction was classified as "within uncertainty" if it fell between the lower and upper 95% confidence limits for the corresponding MPN value. From these confidence intervals, average analytical uncertainty of Colilert is over 27% (IDEXX Laboratories, 2004).

Colilert and MF return units of MPN and CFU per 100 mL, respectively. The difference in units arises from the statistical estimate-derived MPN and direct colony count-derived CFU (ISO, 2012, 2014). Units are agreed to be equivalent and interchangeable, where 1 CFU = 1 MPN (ISO, 2021; Boczek et al., 2023).

3.5. Microbial response

3.5.1. Bench evaluation

Multiple sensor responses to environmental water samples under identical operating conditions were evaluated in the laboratory using a recirculating tank. Three fluorimeters were fully submerged in a plastic 5 gallon bucket initially filled with approximately 7 L of tap water. A pump recirculated the water to produce a well-mixed environment. Water collected from Boulder Creek (intersection of Canyon and 30th) was added to the bucket in 2 L increments at intervals between 30 min and overnight. 500 mL samples were taken before adding new creek water and 20 min after the addition, to allow for adequate mixing and temperature equilibration. Samples were collected with a peristaltic pump, discarding 500 mL before collection for rinsing and to maintain steady water level. Turbidity was measured (Hach 2100N Laboratory Turbidimeter) and each sample was analyzed in triplicate with membrane filtration and Colilert. A total of 67 samples were collected and analyzed.

3.5.2. Field evaluation

Fluorimeters were deployed in several locations in 2025 and complemented with field-collected enumeration data.

Boulder Creek is a tributary of the South Platte River and flows east from the foothills through the City of Boulder and the University of Colorado, covering diverse environmental and land cover settings. Its flow is primarily derived from snow melt and lower-order streams west of the city, producing higher flows in the spring and summer. Boulder has a semi-arid climate with a mean annual rainfall of 19 inches (Murphy, 2006). Segment 2b of Boulder Creek, from 13th Street to the confluence with South Boulder Creek, has been identified on the State of Colorado's 303(d) list of impaired water bodies for nonattainment of water quality standards for *E. coli*. A 303(d) status requires the completion of a total maximum daily load (TMDL) to determine the maximum allowable *E. coli* load to Boulder Creek that will maintain compliance with water quality standards and beneficial uses (Tetra Tech, 2011). Potential sources of *E. coli* are anthropogenic (recreation, leaky sewer lines, failing septic systems) and environmental (runoff containing animal feces, pet waste along the creek, waterfowl and raccoons in storm drains) (Murphy, 2006). The section of Boulder Creek in this study typically has pH ranging from 6.8 to 8.5, turbidity < 10 NTU, hardness between 30 and 1130 mg/L, temperature between 10 and 25 C, and DOC between 2 and 8 mg/L (Murphy et al., 2003).

In the summer of 2025, we conducted a global test of Lumes. These deployments were done with partners in Paris, Boulder, and throughout the Northeastern United States. For this deployment, we were using an earlier version of the Lume hardware that did not include onboard turbidity estimates, so the gradient boosting models developed for this data do not include turbidity as a covariate, though subsequent work highlighted the importance of this data stream (see below).

Fluorimeters were installed at four locations along Boulder Creek for 7 months from March to September 2025. Water samples were collected approximately 5 times per week for 20 weeks between April and August 2025. Samples were plated with one Colilert test and in triplicates for MF. Later, three fluorimeters were installed along Boulder Creek in December 2025 at sites BC-CU, BC-30 and BC-55. The BC-Can site was not used due to frozen water conditions. Samples were collected 4 times daily at each site for 2 weeks. Each sample was plated in triplicates for MF and Colilert.

Four fluorimeters were deployed at multiple locations along the Seine and Marne rivers in the Paris region, during the Summer of 2025 to evaluate performance under highly dynamic urban river conditions. The deployment encompassed sites influenced by variable hydrology, upstream wastewater inputs, and intensive recreational use, and was accompanied by routine grab sampling for laboratory *E. coli* analysis with Colilert.

Across central and the Northeastern United States, four fluorimeters were deployed in urban streams and brackish water. One fluorimeter was deployed in each of the following locations: Calumet River in Chicago, IL; Euclid Creek in Cleveland, OH; Charles River in Boston, MA; Manchester Bay near Boston, MA. The latter was the only deployment in a coastal environment with brackish water. Samples were taken weekly at each site between May and August 2025. Euclid Creek and Manchester Bay sites plated samples with one replicate of Colilert; Calumet and Charles River sites used single replicates of MF.

3.5.3. Analysis of sensor-level performance

After transmission from each fluorimeter over cellular networks, sensor data were extracted from a centralized database and organized into synchronized time series for each deployed instrument. Data streams included fluorescence and turbidity monitor outputs, optical operating parameters (SiPM bias and LED excitation power), internal temperature, and auxiliary optical diagnostics. Measurements were time-stamped at sub-minute resolution and harmonized to a common one-minute temporal grid to enable alignment across data sources. Within each minute, measurements were grouped by sensor identifier and operating condition and aggregated using the median of numeric fields to reduce the influence of transient outliers and electronic noise.

Laboratory *E. coli* measurements were paired with sensor data based on rounded timestamps, at one-minute intervals. When replicate laboratory measurements were available, summary statistics (mean, minimum, and maximum) were retained to represent analytical uncertainty for temperature, turbidity, and fluorescence signals. To support log-scale analysis, non-detect or zero-valued laboratory measurements were assigned a value of 0.1 prior to log transformation.

Continuous relationships between sensor-derived features and laboratory *E. coli* concentrations were evaluated using regression models fit to log-transformed laboratory measurements. Sensor data used in the models included fluorescence, temperature, and sensor-measured turbidity. Models were fit separately for each sensor, and performance was assessed using the coefficient of determination (R^2) and predicted-versus-observed comparisons that incorporated laboratory uncertainty. For operational relevance, laboratory concentrations and corresponding model predictions were grouped into three categories, loosely corresponding to WHO drinking water risk (< 10 low risk, 10–100 medium risk, and > 100 high risk CFU/100 mL), or the threshold categories used by local authorities, and categorical performance was evaluated using confusion matrices and summary metrics including overall accuracy, balanced accuracy, and Cohen's kappa.

All data processing, modeling, and visualization were conducted using the R statistical computing environment. Identical workflows were applied across fluorimeters and deployments to ensure reproducibility and comparability of results.

3.5.4. Machine learning supported global model

All analyses were conducted using a unified data preparation and modeling pipeline implemented in R via the tidymodels framework (Kuhn and Wickham, 2020), with gradient-boosted decision trees fit via the LightGBM engine (Shi et al., 2026). Predictor variables consisted of raw and derived SiPM monitor outputs, water temperature, one-hot encoded site ID, and time since last sensor cleaning. Water temperature was included as a covariate to account for temperature-dependent quenching of fluorescence intensity as well as temperature effects on sensor electronics. These initial deployments did not include onboard turbidity estimates, as that capability was added to the hardware after the summer deployments; subsequent models incorporating turbidity as a covariate are expected to improve performance by accounting for optical attenuation and scattering.

Gradient-boosted decision trees were selected over simpler alternatives (e.g., multiple linear regression, random forests) based on preliminary model comparison. Linear models were unable to capture the nonlinear interactions between fluorescence signals, temperature, and site-specific factors that characterize the TLF–*E. coli* relationship across heterogeneous deployments. Among ensemble methods, LightGBM provided superior cross-validated performance relative to random forests, with faster training times and native support for handling missing values, making it well suited for operational deployment with streaming sensor data.

Continuous model for E. coli. To evaluate quantitative predictive performance, we trained a gradient-boosted regression model with log10-transformed laboratory *E. coli* concentrations as the response variable. Model fitting used a Huber loss function (Huber, 1964), which provides robustness to extreme values while retaining sensitivity to continuous error structure. Sensor observations were aggregated across all deployment sites, with each record uniquely identified by site and timestamp.

The dataset was split temporally, with the most recent 20% of observations at each site reserved as a final holdout test set. The remaining 80% was used for 4-fold cross-validation. Hyperparameters (number of trees, tree depth, learning rate, minimum node size, column subsampling, and row subsampling) were tuned using Bayesian

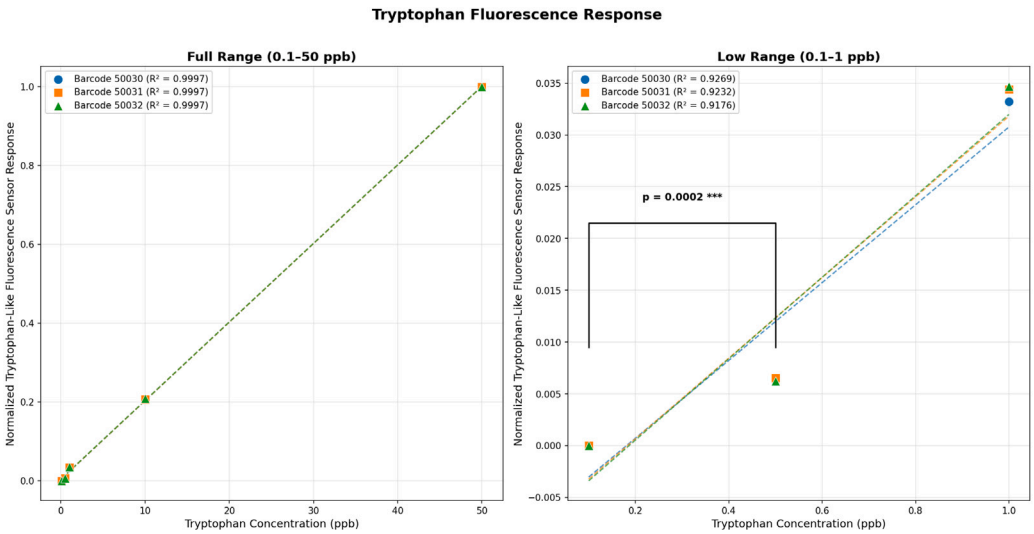

Fig. 3. Normalized tryptophan-like fluorescence (TLF) sensor response as a function of tryptophan concentration for three sensors (barcodes 50030, 50031, 50032). Left panel: full calibration range (0.1–50 ppb) with linear regression fits ($R^2 \approx 0.98$ for all sensors). Right panel: low concentration range (0.1–1 ppb) showing improved linearity ($R^2 > 0.997$). Significance bracket indicates statistically significant difference between 0.1 and 0.5 ppb (paired t-test, $p = 0.0002$). TLF values were min–max normalized within each sensor to enable direct comparison of response profiles.

optimization, initialized from a Latin hypercube design. Early stopping was applied during boosting based on validation RMSE.

To emphasize model performance in the tails of the response distribution, continuous case weights were computed as a function of deviation from the median (scaled by median absolute deviation), and applied during training. After fitting, a linear bias-correction model was estimated on the validation set and applied to all predictions to improve calibration of extreme values. Model performance was summarized using root mean squared error (RMSE), coefficient of determination (R^2), and mean absolute percentage error (MAPE), reported separately for training, validation, and final holdout data.

Classification model (progressive forecasting). A binary classification model was used to assess the ability of the sensor data to reproduce regulatory *E. coli* risk classes in Paris. Laboratory concentrations were discretized into ordinal bins of high and low contamination levels, and the response variable was treated as a binary factor.

Class imbalance was addressed using inverse-frequency class weights, ensuring equal expected contribution of each contamination category to the loss function. Hyperparameter tuning followed the same Bayesian optimization procedure as for the regression model, using binary log-loss as the tuning metric. Classification performance was assessed using overall accuracy and balanced accuracy (mean per-class recall), computed separately for each progressive forecasting step and summarized via confusion matrices.

4. Results

4.1. Tryptophan response

Three tryptophan-like fluorescence (TLF) sensors were calibrated against known tryptophan concentrations ranging from 0.1 to 50 ppb. To account for inherent variability in sensor baseline responses, TLF values were normalized within each sensor using min–max normalization, scaling responses to a 0–1 range based on each sensor's minimum and maximum observed values.

Fig. 3 presents the normalized sensor response as a function of tryptophan concentration across two ranges. The left panel displays the full calibration range (0.1–50 ppb), while the right panel provides a detailed view of the low concentration range (0.1–1 ppb). Linear regression analysis revealed strong linearity across the full measurement range, with coefficients of determination (R^2) of 0.9832, 0.9830, and 0.9838 for sensors 50030, 50031, and 50032, respectively. The consistency of R^2 values across all three sensors demonstrates excellent inter-sensor reproducibility.

At low concentrations (0.1–1 ppb), linearity improved substantially, with R^2 values exceeding 0.997 for all sensors (0.9974, 0.9973, and 0.9970 for sensors 50030, 50031, and 50032, respectively). This enhanced linearity at lower concentrations suggests that the sensors are well-suited for detecting trace-level tryptophan contamination in water quality monitoring applications.

To assess sensor sensitivity at the lower detection limit, a paired t-test was performed comparing normalized responses between 0.1 and 0.5 ppb concentrations across all three sensors. The analysis revealed a statistically significant difference ($p = 0.0002$), indicating that the sensors can reliably discriminate between these two concentration levels. This finding is illustrated graphically in the right panel of Fig. 3, where a significance bracket denotes the statistical comparison between the 0.1 and 0.5 ppb measurement points.

The near-identical normalized response curves across all three sensors underscore the robustness and reproducibility of the TLF measurement approach. Following normalization, sensors exhibited virtually indistinguishable calibration profiles, with normalized responses at each concentration differing by less than 0.001 units between sensors. This high degree of concordance suggests that the normalization procedure effectively compensates for inter-sensor variability, enabling reliable cross-sensor comparisons and potential sensor interchangeability in field applications.

4.2. Turbidity response

Three fluorimeters were tested to evaluate fluorescence sensor (TLF) stability and turbidity sensor (TOF) response to a constant tryptophan concentration (30 ppb) and increasing turbidity from 0 to 100 NTU.

The left panel of Fig. 4 presents the normalized sensor responses as a function of turbidity concentration, ranging from 0–100 NTU. Linear regression analysis indicates excellent linearity from the turbidity (ToF) sensor (blue) across the experimental turbidity range, with a coefficient of determination (R^2) of 0.992. The linear response of the ToF sensor reflects impressive performance of the sensor for turbidity quantification. Fluorescence sensor readings also exhibit strong linearity ($R^2 = 1.000$) in response to increasing turbidity. This indicates a quantifiable linear change in sensor signal under varying turbidity, allowing for turbidity to be controlled and corrected in analysis.

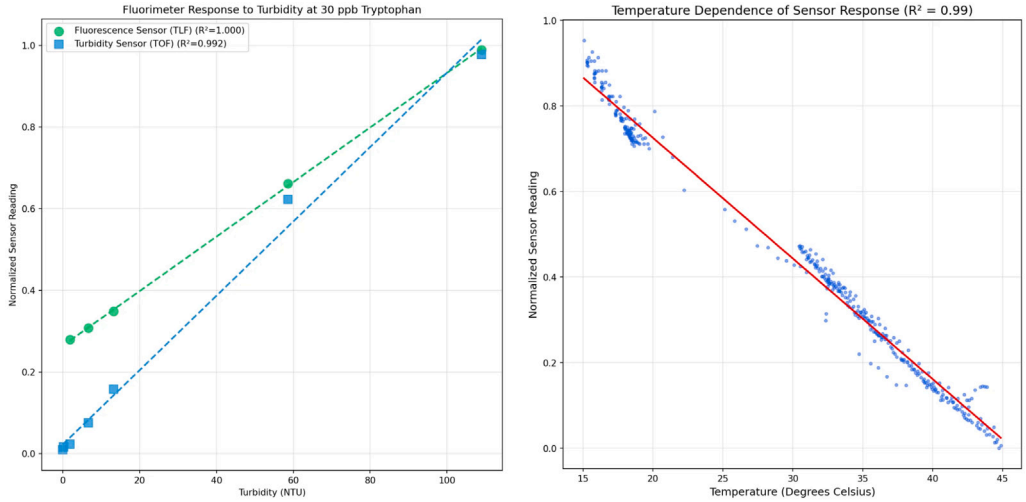

Fig. 4. Left: Fluorescence and turbidity sensor signals signal at constant tryptophan concentration (30 ppb) and increasing turbidity. Right: Temperature dependence of fluorescence sensor signal in ultrapure water. (For interpretation of the references to color in this figure legend, the reader is referred to the web version of this article.)

4.3. Temperature response

Sensors were submerged in ultrapure (DI) water, sealed from potential contaminants, and exposed to diurnal temperature fluctuations in Boulder, CO for three days to test temperature dependence of fluorescence signal.

The right panel of Fig. 4 shows the normalized sensor readings (blue) as a function of temperature, ranging from 15 to 45 °C. A linear regression analysis on sensor readings revealed high linearity, with a coefficient of determination (R^2) of 0.99. This indicates that nearly all variability in sensor readings from ultrapure DI water can be explained by fluctuations in temperature, further revealing the high level of sensor signal temperature-dependence. As such, this provides a strong baseline for sensor readings at varying temperatures, which can therefore be corrected in data analysis.

4.4. Microbial enumeration

A method comparison study was conducted to evaluate the agreement between Colilert (IDEXX Laboratories) and MF techniques for *E. coli* enumeration in water samples (Fig. 5). A total of 161 paired samples were analyzed, with replicate measurements averaged for each method (n=2 for Colilert; n=3 for MF); eight pairs with zero-valued means were excluded from the log-scale analysis, yielding 153 observations. Regression analysis in log-transformed space revealed a positive correlation between the two methods ($r = 0.764$, $R^2 = 0.584$, $p < 0.001$), indicating general agreement in detecting *E. coli* across a wide range of concentrations. The log-space regression slope of 0.63 indicates that MF consistently yielded higher counts than Colilert, particularly at lower concentrations. This systematic bias may reflect fundamental differences between the culture-based MF approach, which enumerates colony-forming units, and the enzyme–substrate Colilert method, which estimates most probable number.

4.5. Microbial response

4.5.1. Bench evaluation

Fig. 6 presents predicted versus observed *E. coli* concentrations for three fluorimeters in the bench-scale bucket test evaluated under identical operating conditions. Across all fluorimeters, predicted concentrations show strong agreement with laboratory-based Colilert reference measurements over approximately three orders of magnitude, spanning low to high fecal contamination levels relevant for both drinking and recreational water monitoring.

Sensor-specific model performance was consistently high, with coefficients of determination (R^2) of 0.84, 0.77, and 0.82 for sensors 50030, 50031, and 50032, respectively, and MAPE of 13%, 15%, and 13%. Data points cluster closely around the 1:1 line, indicating limited systematic bias across the calibrated concentration range. This agreement is particularly strong at moderate to high *E. coli* concentrations (> 10 MPN), which are most relevant for public health decision-making in recreational waters and source water screening.

Over 75% of predictions in this continuous, linear model fell within the uncertainty bounds of the Colilert reference data, defined with 95% confidence for each MPN value (IDEXX Laboratories, 2004) (green points), are concentrated along the 1:1 line, while observations outside this range (orange points) exhibit greater scatter, particularly at the lowest concentrations (< 1–10 MPN). This pattern is consistent across fluorimeters and reflects both increased analytical uncertainty in low-count microbiological measurements and reduced signal-to-noise ratio at the lower detection limits of fluorescence-based sensing. A small number of low-concentration outliers are observed, but these do not dominate overall model performance.

Importantly, model behavior is highly consistent across independently deployed fluorimeters, suggesting good reproducibility of the fluorimeter platform and robustness of the underlying fluorescence–*E. coli* relationship. The absence of strong sensor-specific bias indicates that calibration approaches are transferable and that sensor-to-sensor variability is not a primary driver of prediction error.

Fig. 7 summarizes the categorical classification performance of the fluorimeters in the bench-scale test across three *E. coli* concentration bins (< 10, 10–100, and > 100 MPN), representing low, moderate, and high fecal contamination levels relevant for drinking water screening and recreational water management. Overall classification accuracy was high (accuracy = 0.91), with a balanced accuracy of 0.85 and a Cohen's kappa of 0.60, indicating moderate to substantial agreement beyond chance and robust performance across imbalanced classes.

Correct classifications are strongly concentrated along the diagonal of the confusion matrix, particularly within the 10–100 MPN category, which accounts for the majority of observations. Of the samples observed in this intermediate range, 146 were correctly classified, demonstrating strong model reliability in the concentration band most relevant for routine monitoring and regulatory decision-making. Misclassifications within this category were infrequent and generally

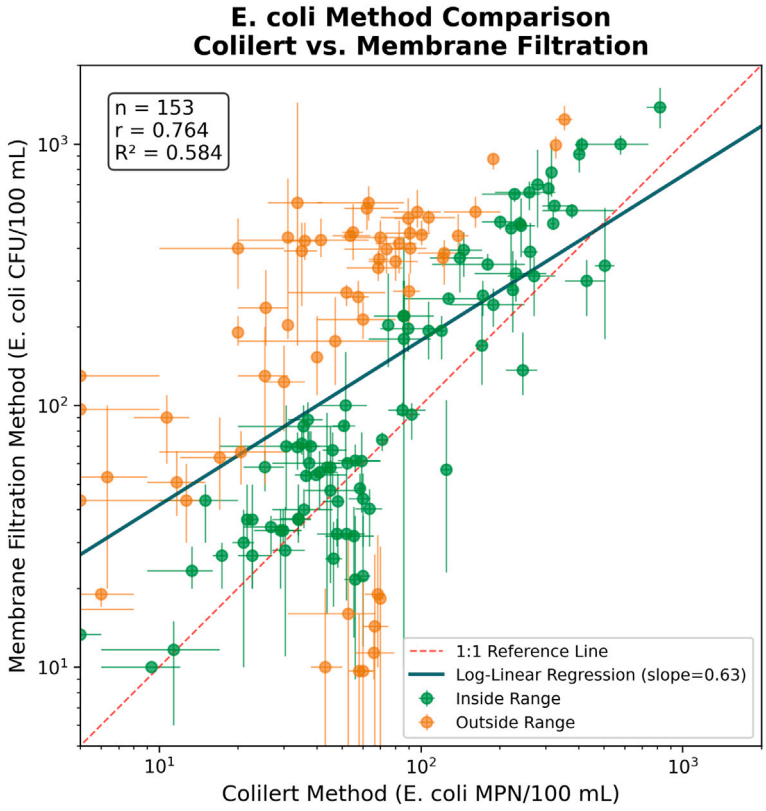

Fig. 5. Comparison of *E. coli* concentrations measured using the Colilert (IDEXX Laboratories) enzyme–substrate method and membrane filtration (MF), shown on logarithmic axes. A total of 153 paired samples were analyzed (8 zero-valued pairs excluded), with replicate measurements averaged for each method (Colilert: $n = 2$; MF: $n = 3$). Error bars represent replicate ranges. Regression in log-transformed space ($r = 0.764$, $R^2 = 0.584$, $p < 0.001$) indicates positive association between methods, with a log-space slope of 0.63 reflecting systematically higher MF counts relative to Colilert, consistent with known methodological differences between colony-forming unit enumeration and most probable number estimation (Harmel et al., 2016; Boczek et al., 2023). Green points denote observations where the two methods agreed within a factor of 3; orange points indicate greater divergence. (For interpretation of the references to color in this figure legend, the reader is referred to the web version of this article.)

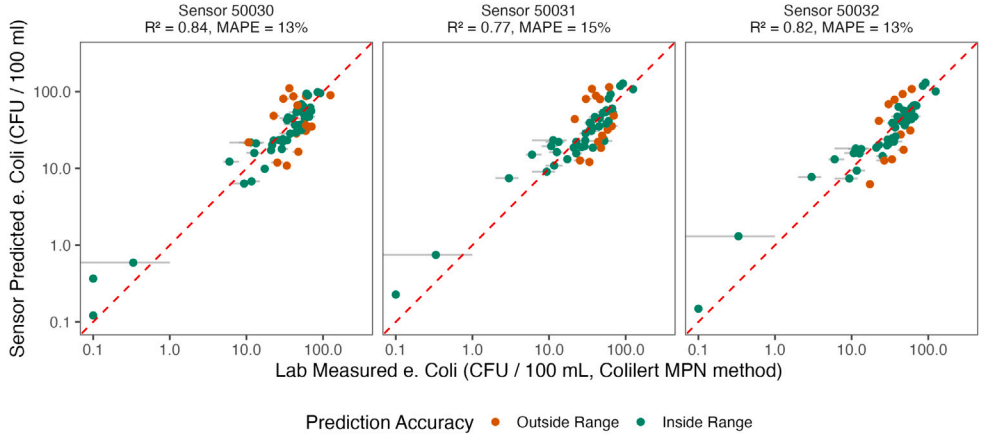

Fig. 6. Predicted versus observed *E. coli* concentrations for three fluorimeters during bench-scale validation under identical operating conditions, shown on logarithmic axes. Laboratory concentrations are reported in MPN/100 mL (Colilert) and have been plotted directly without unit conversion, as MPN and CFU are treated as equivalent for comparison purposes (ISO, 2021; Boczek et al., 2023). Points represent paired sensor–laboratory observations, with the dashed line indicating the 1:1 relationship. Green points denote predictions falling within the analytical uncertainty bounds of the Colilert reference method (95% confidence intervals per IDEXX Laboratories, 2004), while orange points fall outside this range. Per-sensor coefficients of determination ranged from $R^2 = 0.77$ to 0.84, with mean absolute percentage error (MAPE) of 13%–15%. (For interpretation of the references to color in this figure legend, the reader is referred to the web version of this article.)

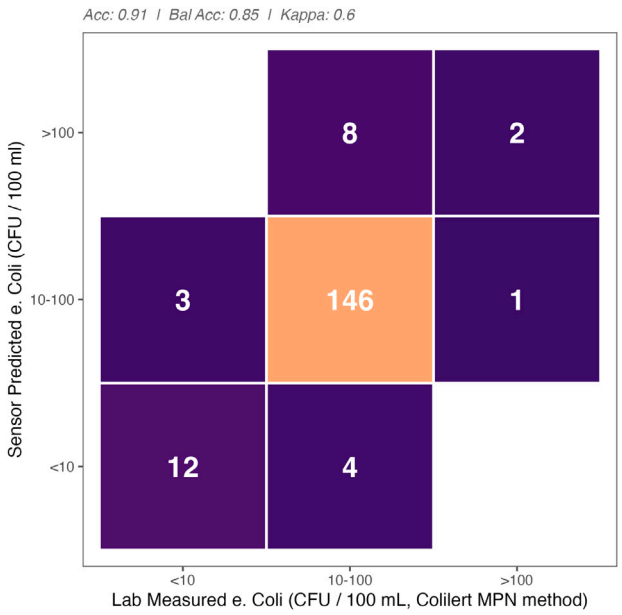

Fig. 7. Confusion matrix summarizing categorical classification performance of the fluorimeters during bench-scale validation. Laboratory *E. coli* concentrations (Colilert MPN method) were grouped into three management-relevant bins (< 10, 10–100, and > 100 MPN per 100 mL). Correct classifications are concentrated along the diagonal, with misclassifications predominantly occurring between adjacent categories. Overall accuracy was 0.91, with balanced accuracy of 0.85 and Cohen's κ of 0.60.

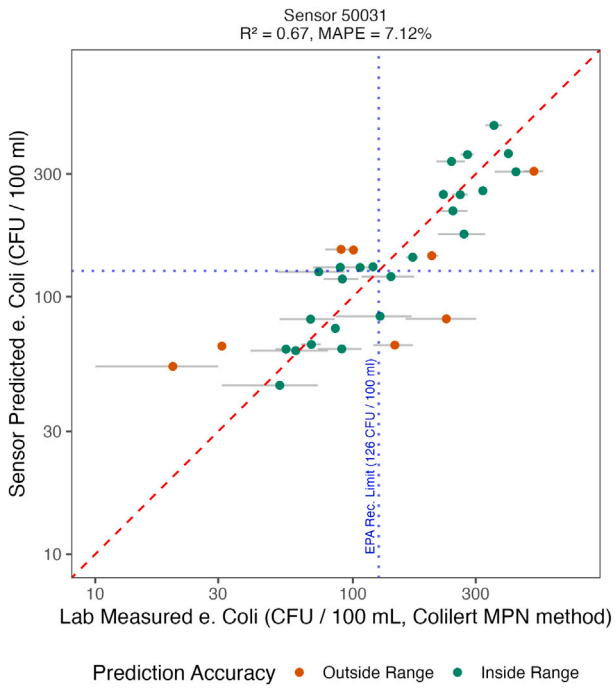

Fig. 8. Comparison of model-estimated and laboratory-measured *E. coli* concentrations for the Boulder Creek test dataset (sensor 50031), shown on logarithmic axes. Laboratory concentrations are reported in MPN/100 mL (Colilert). Horizontal error bars represent 95% confidence intervals of the Colilert MPN values. Dotted blue lines indicate the EPA recreational water quality criterion of 126 CFU/100 mL. Green points denote predictions within the analytical uncertainty bounds; orange points fall outside this range. R^2 = 0.67 with MAPE of 7.12% in log-transformed concentration space. (For interpretation of the references to color in this figure legend, the reader is referred to the web version of this article.)

limited to adjacent bins, reflecting conservative boundary errors rather than large classification failures.

At low concentrations (< 10 MPN), most misclassifications occurred near the lower detection threshold, with some samples classified into the adjacent 10–100 MPN range. This pattern is consistent with both analytical uncertainty inherent in low-count microbiological measurements and reduced signal-to-noise ratios in fluorescence-based sensing at very low concentrations. Importantly, few low-concentration samples were misclassified as high (> 100 MPN), minimizing the risk of false alarms. Similarly, classification performance at high concentrations (> 100 MPN) was strong, with only a small number of samples misclassified into the 10–100 MPN category and minimal confusion with the lowest bin. This asymmetry suggests that the model reliably distinguishes high-risk contamination events while maintaining conservative transitions near category boundaries.

4.5.2. Field evaluation

Field Evaluation is explained here in detail.

4.5.3. Individual sensor level - Boulder Creek

Fig. 8 presents the Boulder Creek model results for one sensor, showing strong agreement between model-estimated and laboratory-measured *E. coli* concentrations across the range of approximately 10 to 400 CFU/100 mL. Similar to the bench-scale results, over 75% of sensor-derived predictions fall within the analytical uncertainty bounds of the Colilert method, indicating that for the majority of samples, differences between predicted and observed values are consistent with the expected error of the reference assay. Quantitative performance under independent test conditions was characterized by a coefficient of determination of $R^2 = 0.67$, indicating that a substantial fraction of observed variability was explained by the model, and a mean absolute percentage error of 7% in log-transformed concentration space. Predicted values generally followed the 1:1 relationship, with deviations occurring primarily at lower concentrations where relative uncertainty in lab-based measurements is greatest. It should be noted that the test dataset for this site contained limited observations below approximately 65 CFU/100 mL, and predictions in this range exhibited greater variability. The apparent agreement at low concentrations should therefore be interpreted cautiously, as the sparse sampling in this range limits the ability to fully characterize model performance near and below typical regulatory thresholds. Overall, these results demonstrate that continuous in-situ measurements provide quantitative estimates of microbial contamination that are statistically consistent with laboratory results for most samples, within the precision limits of the reference method.

4.5.4. Global model

Fig. 9 compares model-estimated and laboratory-measured *E. coli* concentrations across the global dataset using a temporally structured evaluation. The most recent 20% of observations were withheld as an independent holdout set, while earlier data were used for model training and validation. This approach evaluates the model's ability to generalize forward in time, reflecting realistic deployment conditions.

Predicted concentrations show strong agreement with laboratory measurements across more than four orders of magnitude, with comparable performance observed across training and temporally held-out test data. Root mean square error (RMSE) was 0.58 log units for training data and 0.59 log units for the test set. Mean absolute percentage error (MAPE) was 22.49% for training and 18.84% for the test holdout, indicating no performance degradation when predicting unseen, future observations.

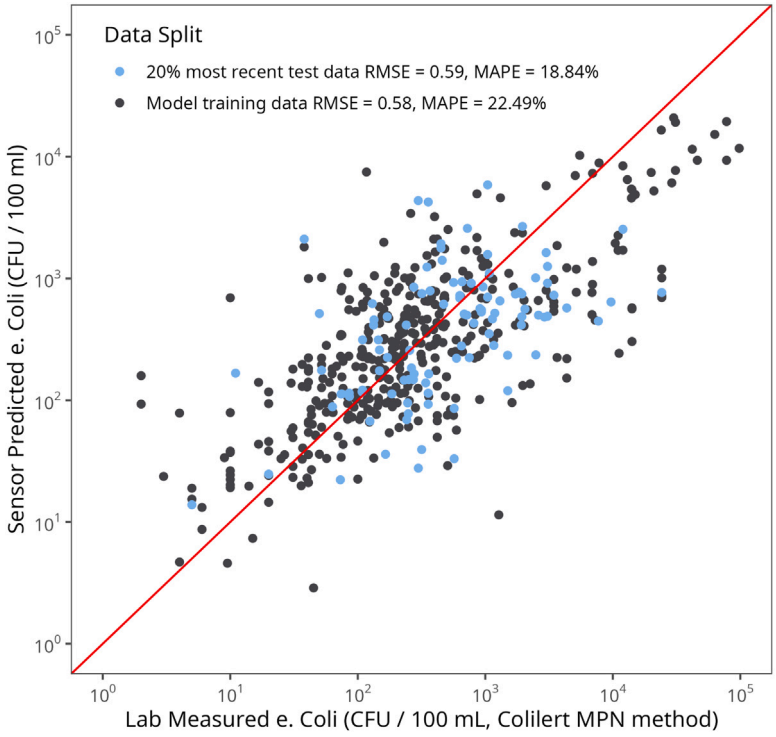

Fig. 9. Comparison of model-estimated and laboratory-measured *E. coli* concentrations across the global dataset using a temporally structured evaluation. The most recent 20% of observations were withheld as an independent holdout test set, with earlier data used for model training and 4-fold cross-validation, to assess forward-in-time generalization. Predicted concentrations show strong agreement with laboratory measurements across more than four orders of magnitude, with comparable performance across training and test data. Root mean square error (RMSE) was 0.58 log units for training and 0.59 log units for the test set, with mean absolute percentage error (MAPE) of 22.49% and 18.84%, respectively. Agreement is strongest at moderate to high concentrations, with greater dispersion at low concentrations reflecting reduced fluorescence signal-to-noise ratios and the inherent uncertainty of culture-based enumeration methods.

Agreement is strongest at moderate to high *E. coli* concentrations, where points cluster near the 1:1 line. Increased dispersion at lower concentrations reflects both reduced fluorescence signal-to-noise ratios and the inherent analytical uncertainty of culture-based enumeration methods. Importantly, errors are not systematically biased across concentration ranges.

It should be noted that the temporal holdout evaluation used here assesses forward-in-time generalization at sites included in training, but does not directly evaluate spatial transferability to entirely unseen sites. When the model is deployed at a new location not represented in the training data, performance may degrade due to site-specific differences in dissolved organic matter composition, background fluorescence, and hydrological regime. As additional deployments are incorporated into the training dataset, spatial generalization is expected to improve; however, initial deployment at a new site may benefit from a brief period of co-located grab sampling to establish site-specific calibration offsets.

4.5.5. Deployment level binary classification model example - Seine, Paris

Binary classification performance further illustrates the operational relevance of continuous measurements, here for the Seine deployments. A total of 310 daily samples across the three Seine swimming docks were collected. Laboratory *E. coli* concentrations were grouped into two management-relevant ranges, ≤900 and >900 CFU/100 mL, reflecting thresholds used for bathing water management. Model training was performed on the first 50% of the Paris dataset, and performance was evaluated on the subsequent 20% of observations to assess forward-in-time generalization under realistic deployment conditions.

During the training period, the model achieved high classification accuracy (95.7%) and balanced accuracy (94.6%), with the majority of samples correctly classified in both categories. Errors were limited and primarily involved misclassification near the category boundary rather than systematic bias toward either class.

Performance remained strong when applied to temporally independent test data. Overall accuracy on the test set was 96.8%, with a balanced accuracy of 94%, indicating no degradation when predicting unseen future observations. As in the training data, misclassifications occurred primarily between adjacent categories, and no systematic failure to identify high-concentration events was observed. This conservative error structure supports the suitability of the approach for operational screening and decision support in dynamic urban river systems (see Fig. 10).

5. Discussion

Overall, the results demonstrate that the fluorimeter platform provides reliable, quantitative estimates of *E. coli* concentrations across ranges most relevant for environmental monitoring, supporting its application for high-frequency microbial water quality assessment in both recreational and source water contexts. Performance limitations are primarily confined to very low concentrations, where conventional culture-based methods themselves exhibit substantial analytical uncertainty. The results further show that the technology effectively classifies microbial contamination into operationally meaningful risk categories with high overall accuracy and limited critical misclassification. Across deployments, model errors are predominantly confined to adjacent concentration categories rather than extreme misclassification between low and high risk. This conservative error structure supports the use of the system for early warning and rapid response applications, particularly

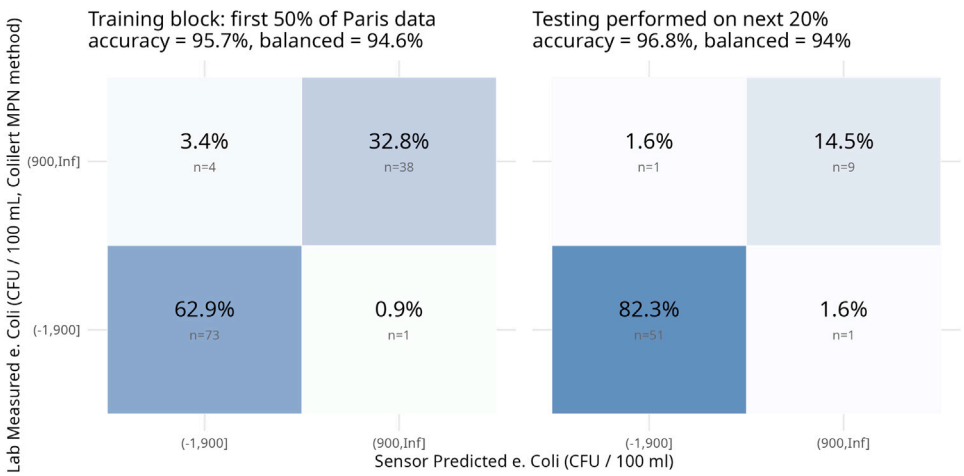

Fig. 10. Binary classification performance for the Paris deployments using a temporally structured evaluation. Laboratory *E. coli* concentrations (Colilert MPN method) were grouped into two operationally relevant ranges (≤900 and >900 CFU/100 mL). Left: training block (first 50% of observations; accuracy 95.7%, balanced accuracy 94.6%). Right: temporally independent test block (next 20%; accuracy 96.8%, balanced accuracy 94%). Cell values show classification percentages and sample counts (*n*). No systematic failure to identify high-concentration events was observed in either split.

in recreational and source water settings where timely identification of moderate-to-high contamination events is essential.

5.1. Reference methods

The method comparison study conducted between EPA approved culture-based methods (Colilert and membrane filtration) for *E. coli* revealed a strong positive correlation between the methods, but not a direct 1:1 relationship of MPN/100 mL (Colilert) to CFU/100 mL (MF). This indicates divergent results for *E. coli* enumeration within accepted culture-based methods, where our comparison found membrane filtration to consistently estimate concentrations up to 45% greater than Colilert on average. These error bounds, which often go unrecognized for culture-based methods, are larger in magnitude, but overall consistent with manufacturer statements and previous literature (Harmel et al., 2016; IDEXX Laboratories, 2004). Variability within and between culture-based methods presents a challenge for building sensor models and comparing performance. Ground-truth data should be visualized with horizontal error bars to reflect known uncertainty of concentrations. When accounting for inherent error of lab-based methods in our models, sensor performance increases, providing a more holistic evaluation of sensor performance and capability.

5.2. Sensitivity

This study demonstrates the ability to reliably distinguish in the sub-ppb range dissolved tryptophan under fixed operating conditions, placing the system among the most sensitive in-situ TLF instruments reported to date. This performance exceeds the manufacturer-stated detection limits of many widely deployed commercial fluorometers and extends effective measurement capability below the concentration ranges most commonly discussed in the TLF–microbial contamination literature.

For example, the Turner Designs Cyclops-7 and the TriOS microFlu-V2, when configured for TLF, both report minimum detection limits on the order of 3 $\mu g\ L^{-1}$ (3 ppb). These instruments are widely used for tracking wastewater influence and organic matter dynamics, but are not specified to resolve sub-ppb concentrations. Higher-sensitivity UV fluorimeters are available; the Chelsea Technologies Group UviLux reports a nominal tryptophan detection limit of approximately 0.02 $\mu g\ L^{-1}$ under controlled conditions. However, published field applications rarely demonstrate repeatable discrimination between near-zero concentrations and ~0.1 ppb across multiple fluorimeters due to background fluorescence, electronic noise, and environmental variability (Nowicki et al., 2019; Ward et al., 2020; Khamis et al., 2015).

A structured comparison of detection limits, dynamic range, and other specifications across commercially available TLF instruments is provided in Table 1.

In this context, the consistent separation observed here between 0.1 and 0.4 ppb across three fluorimeters is notable. Rather than relying on single-instrument detection limits, these results demonstrate reproducible low-end resolution under identical operating conditions. Sensitivity in this range may enable earlier detection of emerging contamination and improved characterization of low-background waters, particularly in source water and upstream monitoring applications.

5.3. Quantification

This work builds directly on Bedell et al. (2022), which introduced an earlier-generation TLF sensor and evaluated its performance using categorical classification against World Health Organization drinking water risk thresholds. That study employed a simpler hardware platform without onboard turbidity or temperature compensation, used a limited number of deployment sites, and framed TLF exclusively as a risk-based screening tool rather than a quantitative predictor of *E. coli* concentration. The present study advances that earlier work in several specific ways: (1) a redesigned fluorimeter with improved optical sensitivity, onboard turbidity and temperature sensing, and enhanced calibration workflows; (2) expansion from site-specific categorical models to both site-specific continuous regression and a global multi-site machine learning framework; (3) a substantially larger and more geographically diverse dataset spanning laboratory, bench-scale, and multi-continent field deployments; and (4) temporal holdout evaluation strategies that more rigorously assess forward-in-time predictive performance.

The present results demonstrate a clear advancement in quantitative capability. Across three fluorimeters, predicted *E. coli* concentrations show strong agreement with laboratory-based Colilert measurements, with coefficients of determination ranging from 0.79 to 0.83 over approximately three orders of magnitude. These results indicate that refinements in sensor design, calibration, and model formulation now permit semi-quantitative estimation of *E. coli* concentrations, particularly at moderate to high contamination levels.

These promising lab results were supported by a global real-world deployment in a wide range of conditions, near-shore ocean, large, highly contaminated rivers, and small intermittently contaminated

Table 1
Comparison of in-situ tryptophan-like fluorescence (TLF) instruments. Detection limits reflect manufacturer-stated specifications under controlled laboratory conditions unless otherwise noted. Sensor-only instruments require separate procurement of a data logger, telemetry hardware, enclosure, and data management platform to achieve continuous field monitoring.

Instrument	LOD (ppb)	Range (ppb)	Ex/Em (nm)	Anti-fouling	Approx. Cost
Turner Designs Cyclops-7[a]	3	0–5000	280/350	No	$4–10k[i]
Turner Designs C-FLUOR[b]	3	0–5000	280/350	No	$4–10k[i]
Chelsea Technologies UviLux	0.02[c]	0–5000[d]	280/350	Optional	$4–10k[i]
TriOS microFlu-V2	3	0–5000	280/350	Coated window	$4–10k[i]
Proteus Instruments[e]	3	0–5000	280/350	Wiper option	~$28k[j]
Virridy Lume (this study)	<0.1[f]	0.1–50[g]	273/350	No[h]	$2400/yr[k]

[a] Discontinued; replaced by C-FLUOR.

[b] Successor to Cyclops-7; titanium housing rated to 2000 m.

[c] Nominal detection limit under controlled conditions; field applications report higher practical limits (Nowicki et al., 2019; Ward et al., 2020).

[d] Calibrated in quinine sulfate units; ppb equivalent is approximate.

[e] Multiparameter platform integrating a Turner Designs fluorometer for TLF; specifications reflect the embedded Turner probe.

[f] Reproducible discrimination between 0.1 and 0.5 ppb across three fluorimeters ($p = 0.0002$); empirical detection threshold based on lowest calibration standard producing a statistically significant response.

[g] Laboratory-validated calibration range; field models span wider concentration ranges.

[h] Manual cleaning at 1–2 week intervals.

[i] Sensor-only purchase price; published estimates for commercial submersible TLF fluorometers range from $4000 to $10,000 (Bedell et al., 2022). Deploying these sensors for continuous monitoring additionally requires a data logger, cellular or radio telemetry, weatherproof enclosure, and cloud data platform, which can equal or exceed the cost of the sensor itself.

[j] Multiparameter platform including telemetry; typical 6-parameter configuration (TLF, turbidity, temperature, conductivity, pH, dissolved oxygen) with data logging and communications.

[k] All-inclusive annual rental including sensor hardware (TLF, turbidity, temperature), integrated cellular telemetry, cloud-based data platform, and remote diagnostics; no additional data logger, modem, or software subscription required.

creeks. Across all of these diverse deployments, we achieved a 20% MAPE for a continuous model, on time-blocked holdout data. This deployment did not include turbidity and we expect future versions of a similar approach will have substantial performance improvements.

Additionally, while laboratory turbidity testing demonstrated a linear sensor response using standardized formazin suspensions, real-world suspended sediments exhibit heterogeneous optical properties depending on particle composition, size distribution, and mineralogy. Fine-grained sediments such as clay and silt scatter and absorb light differently than the synthetic standards used here, and rapidly changing turbidity during storm events may introduce transient optical interference that is not fully captured by the current correction approach. Field deployments in Boulder Creek, which experiences episodic sediment pulses, did not reveal systematic turbidity-driven bias in the concentration ranges observed, but performance under sustained high-turbidity conditions (>100 NTU) with natural sediment loads remains to be fully characterized.

Across all tests, consistent with prior findings, uncertainty remains greatest at very low concentrations (<10 MPN), where both fluorescence signal-to-noise ratios and laboratory enumeration precision are limited. Rather than contradicting earlier conclusions, these results refine them by clarifying the concentration ranges over which quantitative prediction is feasible and those where categorical screening remains the most appropriate application.

5.4. Classification

Our combined studies in lab, local, and global deployments, demonstrates strong performance in classifying contamination at concentrations most relevant for public health protection. In the present study, grouping concentrations into three operationally meaningful bins (<10, 10–100, and >100 MPN) yielded an overall accuracy of 0.91 and balanced accuracy of 0.77. Misclassifications were overwhelmingly confined to adjacent categories, minimizing the likelihood of failing to identify potentially hazardous conditions. With more data and higher ranges of E. Coli, a simple classification model at relevant thresholds in Paris performed even better, with more than 90% accuracy.

Feature importance analysis of the gradient-boosted model confirmed that fluorescence-derived variables (raw and temperature-corrected SiPM outputs) were the dominant predictors of *E. coli* concentration, accounting for the majority of model gain. Water temperature and time since last cleaning contributed secondary but meaningful predictive power, consistent with known temperature quenching effects and gradual signal attenuation from biofouling. Site identifiers contributed modestly, primarily capturing differences in background DOM and baseline fluorescence characteristics across deployments. A full SHAP (SHapley Additive exPlanations) analysis is planned for a follow-up study incorporating the expanded dataset with onboard turbidity measurements, which will enable more detailed attribution of model behavior across environmental gradients.

Improvements in sensor optics, electronics, and calibration workflows appear to have reduced sensor-specific bias and improved reproducibility across deployments. Predictive performance was consistent across independently deployed fluorimeters, indicating that while environmental correction remains important, the system is increasingly robust to site- and sensor-specific variability. This represents an important step toward scalable deployment in heterogeneous surface water environments.

5.5. Interferences and specificity

TLF is not exclusively specific to fecal contamination; non-fecal sources of tryptophan-like fluorophores, including algal exudates, terrestrial dissolved organic matter (DOM) from leaf litter and soil runoff, and humic-like substances, can contribute to the measured fluorescence signal. High concentrations of humic DOM can also cause inner filter effects (IFE), where absorption of excitation or emission light attenuates the measured fluorescence intensity. In the deployments presented here, the machine learning model partially accounts for these interferences through inclusion of site-specific identifiers and temporal features, which implicitly capture background DOM variability at each location. However, events that introduce anomalous DOM loads — such as heavy rainfall flushing terrestrial organic matter into the water column, or algal blooms producing elevated protein-like fluorescence — can produce false-positive *E. coli* predictions. In the current

dataset, elevated false-positive rates were most frequently associated with storm events that produced rapid increases in turbidity and DOM loading simultaneously. Explicit correction for IFE was not applied in this study, as absorption measurements at excitation and emission wavelengths were not collected in situ; future sensor iterations incorporating absorbance measurements or complementary fluorescence channels (e.g., humic-like fluorescence at 370/460 nm) could enable real-time IFE correction and improved discrimination between fecal and non-fecal fluorescence sources.

5.6. Comparison

Several commercial instruments measuring TLF have been applied in studies relating fluorescence to microbial contamination, including the Turner Designs Cyclops series, Chelsea Technologies Group UviLux, and TriOS microFlu. Reported quantitative relationships between TLF and microbial indicators in these studies typically exhibit coefficients of determination in the range of 0.5–0.8 and are often sensitive to environmental interferences such as turbidity and temperature (Khamis et al., 2015; Ward et al., 2021).

In comparison, the continuous fluorescence measurements and modeling framework presented here achieve similarly strong or stronger quantitative agreement and categorical classification performance across multiple, hydrologically dynamic field deployments, with reproducible behavior across independently deployed fluorimeters. These results suggest that advances in low-end sensitivity, calibration, and modeling contribute meaningfully to improved robustness and transferability.

5.7. Biofouling and maintenance

Biofouling of the optical window is a universal challenge for in-situ optical sensors and represents a practical constraint on deployment duration and data quality. In this study, field deployments ranged from two weeks to seven months in duration. The sensor does not currently incorporate active anti-fouling mechanisms such as mechanical wipers or copper-based coatings. Instead, sensor maintenance was performed on a regular schedule, with cleaning events logged and recorded. Time since last cleaning was included as a predictor variable in the machine learning model, allowing the algorithm to partially compensate for gradual signal drift associated with biofilm accumulation. In practice, cleaning intervals of one to two weeks were sufficient to maintain data quality at most sites, though sites with high nutrient loading or warm water temperatures required more frequent maintenance. Future hardware iterations may incorporate mechanical or chemical anti-fouling systems to extend unattended deployment intervals and reduce maintenance burden, which will be important for scaling to operational monitoring networks.

5.8. Application

Partner agencies currently use real-time fluorescence-derived microbial estimates to support recreation advisories, operational decision-making, and public-facing communication. Continuous data streams allow managers to identify rapid contamination events associated with storms, wastewater infrastructure impacts, or upstream disturbances, and to distinguish transient events from background variability. This temporal context supports more informed decisions regarding closures, advisories, and reopening timing, reducing both unnecessary precautionary actions and missed high-risk exposure periods.

By translating continuous measurements into operational risk categories aligned with existing thresholds, the platform functions as an early-warning and screening tool that prioritizes confirmatory sampling and supports transparent communication of uncertainty. As climate-driven hydrologic variability and recreational water use increase, the ability to augment traditional monitoring with real-time microbial data represents a meaningful advancement for public health protection.

6. Conclusions

This study demonstrates that continuous, in-situ measurement of TLF can support both quantitative estimation and categorical classification of microbial contamination across environmentally relevant concentration ranges. Relative to prior work, the results show improved quantitative agreement with laboratory-based *E. coli* enumeration, enhanced classification accuracy at operational thresholds, and increased reproducibility across independently deployed fluorimeters. Together, these findings indicate that the platform provides a scalable, robust tool for high-frequency microbial water quality monitoring. When integrated with laboratory confirmation and existing regulatory frameworks, continuous TLF-based sensing can enhance protection of public health in both recreational waters and drinking water source systems by enabling timely identification of transient contamination events that are otherwise difficult to detect.

CRediT authorship contribution statement

Whitney Knopp: Writing – original draft, Methodology, Investigation, Formal analysis, Data curation, Conceptualization. **Joshua Klaus:** Writing – review & editing, Methodology, Investigation, Data curation. **Danny Wilson:** Writing – review & editing, Validation, Methodology, Conceptualization. **Michael J. Vlah:** Writing – review & editing, Formal analysis, Data curation, Conceptualization. **Matthew R.V. Ross:** Writing – original draft, Supervision, Project administration, Methodology, Investigation, Funding acquisition, Formal analysis, Data curation, Conceptualization. **Evan Thomas:** Writing – original draft, Visualization, Supervision, Resources, Project administration, Methodology, Investigation, Funding acquisition, Formal analysis, Data curation, Conceptualization.

Declaration of generative AI and AI-assisted technologies in the manuscript preparation process

During the preparation of this work the authors used Claude and ChatGPT in order to refine and summarize figures. After using this tool/service, the authors reviewed and edited the content as needed and take full responsibility for the content of the published article.

Declaration of competing interest

The authors declare that they have no known competing financial interests or personal relationships that could have appeared to influence the work reported in this paper.

Acknowledgments

This work was supported by the National Science Foundation Convergence Accelerator (Award #24C0011), The National Science Foundation ASCEND Engine (Award #NSF-2315760), and the National Aeronautics and Space Administration, United States (Award #80NSSC 24K0998). The authors thank their collaborating partners Michael Lawlor from the City of Boulder, Françoise Lucas from the Université Paris-Est Créteil, Jean-Marie Mouchel from the Sorbonne Université, Marion Delarbre from the City of Paris, Marielena Lima from the Charles River Watershed Authority, Melissa Pierce and Tyler Stephen from Current Water, Jillian Knittle and Christina Miller from the Northeast Ohio Regional Sewer District, Natalie Van Scyoc and Jeff Pu from the Cleveland Water Alliance, and Ray Ozzie from Blues Wireless.

Data availability

The dataset and modeling code used in this study are publicly available on GitHub at https://github.com/SweetSenseInc/lume_natural_waters_paper.

References

Adams, M.R., Grubb, S.M., Hamer, A., Clifford, M.N., 1990. Colorimetric enumeration of Escherichia coli based on beta-glucuronidase activity. Appl. Environ. Microbiol. 56, 2021–2024. http://dx.doi.org/10.1128/aem.56.7.2021-2024.1990, URL: https://journals.asm.org/doi/10.1128/aem.56.7.2021-2024.1990.

Baker, A., Elliott, S., Lead, J.R., 2007. Effects of filtration and pH perturbation on freshwater organic matter fluorescence. Chemosphere 67, 2035–2043. http://dx.doi.org/10.1016/j.chemosphere.2006.11.024.

Bedell, E., Harmon, O., Fankhauser, K., Shivers, Z., Thomas, E., 2022. A continuous, in-situ, near-time fluorescence sensor coupled with a machine learning model for detection of fecal contamination risk in drinking water: Design, characterization and field validation. Water Res. 220, 118644. http://dx.doi.org/10.1016/J.WATRES.2022.118644.

Benjamin, L., Atwill, E.R., Jay-Russell, M., Cooley, M., Carychao, D., Gorski, L., Mandrell, R.E., 2013. Occurrence of generic Escherichia coli, E. coli O157 and salmonella spp. in water and sediment from leafy green produce farms and streams on the central California coast. Int. J. Food Microbiol. 165, 65–76. http://dx.doi.org/10.1016/j.ijfoodmicro.2013.04.003.

Boczek, L., Herrmann, R., Resek, E., Richman, T., 2023. Pathogens and Vector Attraction in Sewage Sludge. Technical Report, U.S. Environmental Protection Agency, Washington, DC.

Collier, S.A., Deng, L., Adam, E.A., Benedict, K.M., Beshearse, E.M., Blackstock, A.J., Bruce, B.B., Derado, G., Edens, C., Fullerton, K.E., Gargano, J.W., Geissler, A.L., Hall, A.J., Havelaar, A.H., Hill, V.R., Hoekstra, R.M., Reddy, S.C., Scallan, E., Stokes, E.K., Yoder, J.S., Beach, M.J., 2021. Estimate of burden and direct healthcare cost of infectious waterborne disease in the United States. Emerg. Infect. Dis. 27, 140–149. http://dx.doi.org/10.3201/eid2701.190676.

Craun, G.F., Calderon, R.L., Craun, M.F., 2005. Outbreaks associated with recreational water in the United States. Int. J. Environ. Health Res. 15, 243–262. http://dx.doi.org/10.1080/09603120500155716.

EPA, 2012. Office of Water 820-F-12-058 Recreational Water Quality Criteria. Technical Report, U.S. Environmental Protection Agency.

EPA, 2016. Online Source Water Quality Monitoring: For Water Quality Surveillance and Response Systems. Technical Report, U. S. Environmental Protection Agency.

EPA, 2018. National Primary Drinking Water Regulations; Expedited Approval of Alternative Test Procedures for the Analysis of Contaminants Under the Safe Drinking Water Act; Analysis and Sampling Procedures. Technical Report, U. S. Envrionmental Protection Agency.

EPA, 2023. Method 1103.2: Escherichia Coli (E. Coli) in Water by Membrane Filtration Using Membrane-Thermotolerant Escherichia Coli Agar (mTEC). Technical Report, US. Environmental Protection Agency, Washington, URL: www.epa.gov.

European Parliament and Council of the European Union, 2006. Directive 2006/7/EC of the European parliament and of the council of 15 february 2006 concerning the management of bathing water quality and repealing directive 76/160/EEC. p. 13.

Hamoudi, A., Jeuland, M., Lombardo, S., Patil, S., Pattanayak, S.K., Rai, S., 2012. The effect of water quality testing on household behavior: Evidence from an experiment in rural India. Am. J. Trop. Med. Hyg. 87, 18–22. http://dx.doi.org/10.4269/ajtmh.2012.12-0051.

Harmel, R.D., Cooper, R.J., Slade, R.M., Haney, R.L., Arnold, J.G., 2006. Cumulative uncertainty in measure streamflow and water quality data for small watersheds. Trans. ASABE 49, 689–701. http://dx.doi.org/10.13031/2013.20488.

Harmel, R.D., Hathaway, J.M., Wagner, K.L., Wolfe, J.E., Karthikeyan, R., Francesconi, W., McCarthy, D.T., 2016. Uncertainty in monitoring E. coli concentrations in streams and stormwater runoff. J. Hydrol. 534, 524–533. http://dx.doi.org/10.1016/j.jhydrol.2016.01.040.

Hope, R., 2024. Four billion people lack safe water. Sci. (New York, N.Y.) 385, 708–709. http://dx.doi.org/10.1126/science.adr3271.

Huber, P.J., 1964. Robust estimation of a location parameter. Ann. Math. Stat. 35 (1), 73–101. http://dx.doi.org/10.1214/aoms/1177703732, URL: https://doi.org/10.1214/aoms/1177703732.

IDEXX Laboratories, 2004. Quanti-Tray/2000 MPN Table (per 100mL) with 95% Confidence Limits. Technical Report, IDEXX Laboratories.

ISO, 2012. ISO 9308-2:2012 Water Quality - Enumeration of Escherichia Coli and Coliform Bacteria - Part 2: Most Probable Number Method. Technical Report, International Organization for Standardization, Geneva.

ISO, 2014. ISO 9308-1:2014. Technical Report, International Organization for Standardization, Geneva.

ISO, 2021. Water Quality - Vocabulary ISO6107:2021. Technical Report, International Organization for Standardization, Geneva.

Jalan, J., Somanathan, E., 2008. The importance of being informed: Experimental evidence on demand for environmental quality. J. Dev. Econ. 87, 14–28. http://dx.doi.org/10.1016/j.jdeveco.2007.10.002.

Jariyasopit, N., Khoomrung, S., 2023. Mass spectrometry-based analysis of gut microbial metabolites of aromatic amino acids. Comput. Struct. Biotechnol. J. 21, 4777–4789. http://dx.doi.org/10.1016/j.csbj.2023.09.032.

Jones, E.R., Bierkens, M.F.P., Wanders, N., Sutanudjaja, E.H., van Beek, L.P.H., van Vliet, M.T.H., 2023. DynQual v1.0: A high-resolution global surface water quality model. pp. 4481–4500. http://dx.doi.org/10.5194/gmd-2022-222, URL: https://gmd.copernicus.org/articles/16/4481/2023/gmd-16-4481-2023-discussion.html.

Jones, E.R., Graham, D.J., van Griensven, A., Flörke, M., van Vliet, M.T., 2024. Blind spots in global water quality monitoring. Environ. Res. Lett. 19, http://dx.doi.org/10.1088/1748-9326/ad6919.

Khamis, K., Sorensen, J.P., Bradley, C., Hannah, D.M., Lapworth, D.J., Stevens, R., 2015. In situ tryptophan-like fluorometers: Assessing turbidity and temperature effects for freshwater applications. Environ. Sci.: Process. Impacts 17, 740–752. http://dx.doi.org/10.1039/c5em00030k.

Kuhn, M., Wickham, H., 2020. Tidymodels: a collection of packages for modeling and machine learning using tidyverse principles. URL: https://www.tidymodels.org.

Murphy, S.F., 2006. State of the Watershed : Water Quality of Boulder Creek, Colorado. U.S. Geological Survey, p. 34.

Murphy, S.F., Verplanck, P.L., Barber, L.B., 2003. Comprehensive Water Quality of the Boulder Creek Watershed, Colorado, During High-Flow and Low-Flow Conditions, 2000. Technical Report, U.S. Geological Survey, Denver.

Nowicki, S., Lapworth, D.J., Ward, J.S., Thomson, P., Charles, K., 2019. Tryptophan-like fluorescence as a measure of microbial contamination risk in groundwater. Sci. Total Environ. 646, 782–791. http://dx.doi.org/10.1016/j.scitotenv.2018.07.274.

Offenbaume, K.L., Bertone, E., Stewart, R.A., 2020. Monitoring approaches for faecal indicator bacteria in water: Visioning a remote real-time sensor for e. coli and enterococci. Water (Switzerland) 12, http://dx.doi.org/10.3390/w12092591.

Okyere, C.Y., Pangaribowo, E.H., Asante, F.A., von Braun, J., 2017. The Impacts of Household Water Quality Testing and Information on Safe Water Behaviors: Evidence from a Randomized Experiment in Ghana. Technical Report, URL: https://ssrn.com/abstract=2955038https://ssrn.com/abstract=2955038.

Rice, E.W., Allen, M.J., Edberg, S.C., 0000. Identification of Escherichia Coli by Colilert B-Glucuronidase Assay: Sensitivity, Specificity, and Implications for Water Testing. Technical Report, American Water Works Association Research Foundation.

Schilling, K.E., Zhang, Y.K., Hill, D.R., Jones, C.S., Wolter, C.F., 2009. Temporal variations of Escherichia coli concentrations in a large Midwestern river. J. Hydrol. 365 (1–2), http://dx.doi.org/10.1016/j.jhydrol.2008.11.029.

Shi, Y., Ke, G., Soukhavong, D., Lamb, J., Meng, Q., Finley, T., Wang, T., Chen, W., Ma, W., Ye, Q., Liu, T.Y., Titov, N., Cortes, D., 2026. lightgbm: Light gradient boosting machine. URL: https://github.com/Microsoft/LightGBM, R package version 4.6.0.99.

Sorensen, J.P., Baker, A., Cumberland, S.A., Lapworth, D.J., MacDonald, A.M., Pedley, S., Taylor, R.G., Ward, J.S., 2018. Real-time detection of faecally contaminated drinking water with tryptophan-like fluorescence: defining threshold values. Sci. Total Environ. 622–623, 1250–1257. http://dx.doi.org/10.1016/J.SCITOTENV.2017.11.162.

Sorensen, J.P., Diaw, M.T., Pouye, A., Roffo, R., Diongue, D.M., Faye, S.C., Gaye, C.B., Fox, B.G., Goodall, T., Lapworth, D.J., MacDonald, A.M., Read, D.S., Ciric, L., Taylor, R.G., 2020. In-situ fluorescence spectroscopy indicates total bacterial abundance and dissolved organic carbon. Sci. Total Environ. 738, 139419. http://dx.doi.org/10.1016/J.SCITOTENV.2020.139419.

Sorensen, J.P., Lapworth, D.J., Marchant, B.P., Nkhuwa, D.C., Pedley, S., Stuart, M.E., Bell, R.A., Chirwa, M., Kabika, J., Liemisa, M., Chibesa, M., 2015. In-situ tryptophan-like fluorescence: A real-time indicator of faecal contamination in drinking water supplies. Water Res. 81, 38–46. http://dx.doi.org/10.1016/j.watres.2015.05.035.

Tetra Tech, 2011. Boulder Creek, Colorado Segment 2b: From 13th Street to the Confluence with South Boulder Creek Total Maximum Daily Load Escherichia coli City of Boulder. Technical Report.

Tiwari, A., Oliver, D.M., Bivins, A., Sherchan, S.P., Pitkänen, T., 2021. Bathing water quality monitoring practices in europe and the united states. Int. J. Environ. Res. Public Health 18, http://dx.doi.org/10.3390/ijerph18115513.

Trent, M., Dreibelbis, R., Bir, A., Tripathi, S.N., Labhasetwar, P., Nagarnaik, P., Loo, A., Bain, R., Jeuland, M., Brown, J., 2018. Access to household water quality information leads to safer water: A cluster randomized controlled trial in india. Environ. Sci. Technol. 52, 5319–5329. http://dx.doi.org/10.1021/acs.est.8b00035.

UNICEF, 2023. UNICEF Target Product Profile Rapid Water Quality Detection Tests. Technical Report, United Nations Children's Fund.

U.S. Environmental Protection Agency, 2024. 40 CFR Part 141—National Primary Drinking Water Regulations. Code of Federal Regulations, URL: https://www.ecfr.gov/current/title-40/part-141, Authorized by the Safe Drinking Water Act, 42 U.S.C. §300f et seq.

Verhougstraete, M., Sexton, J., 2015. Recreational water contamination. In: Routledge Handbook of Water and Health. Taylor & Francis, London and New York: Routledge.

van Vliet, M.T., Thorslund, J., Strokal, M., Hofstra, N., Flörke, M., Macedo, H.E., Nkwasa, A., Tang, T., Kaushal, S.S., Kumar, R., van Griensven, A., Bouwman, L., Mosley, L.M., 2023. Global river water quality under climate change and hydroclimatic extremes. Nat. Rev. Earth Environ. 4, 687–702. http://dx.doi.org/10.1038/s43017-023-00472-3.

Walker, D., Baumgartner, D., Gerba, C., Fitzsimmons, K., 2019. Surface water pollution. In: Environmental and Pollution Science. Elsevier, pp. 261–292. http://dx.doi.org/10.1016/b978-0-12-814719-1.00016-1.

Ward, J.S., Lapworth, D.J., Read, D.S., Pedley, S., Banda, S.T., Monjerezi, M., Gwengweya, G., MacDonald, A.M., 2020. Large-scale survey of seasonal drinking water quality in malawi using in situ tryptophan-like fluorescence and conventional water quality indicators. Sci. Total Environ. 744, http://dx.doi.org/10.1016/j.scitotenv.2020.140674.

Ward, J.S., Lapworth, D.J., Read, D.S., Pedley, S., Banda, S.T., Monjerezi, M., Gwengweya, G., MacDonald, A.M., 2021. Tryptophan-like fluorescence as a high-level screening tool for detecting microbial contamination in drinking water. Sci. Total Environ. 750, 141284. http://dx.doi.org/10.1016/J.SCITOTENV.2020.141284.

WHO, 2003. Chlorine in Drinking-Water: Background Document for Development of WHO Guidelines for Drinking-Water Quality. Technical Report, World Health Organization, Geneva.

WHO, 2022. Guidelines for Drinking-Water Quality: Fourth Edition Incorporating the First and Second Addenda. Technical Report, World Health Organization, Geneva.